Cancer Science
Japanese Cancer Association JCA
Open Access

Role of hemoglobin and transferrin in multi-wall carbon nanotube-induced mesothelial injury and carcinogenesis

Yue Wang,[1] Yasumasa Okazaki,[1] Lei Shi,[1] Hiro Kohda,[1] Minoru Tanaka,[2] Kentaro Taki,[2] Tomoki Nishioka,[3] Tasuku Hirayama,[4] Hideko Nagasawa,[4] Yoriko Yamashita[1] and Shinya Toyokuni[1]

[1]Department of Pathology and Biological Responses; [2]Division for Medical Research Engineering; [3]Department of Cellular Pharmacology, Nagoya University Graduate School of Medicine, Nagoya; [4]Laboratory of Pharmaceutical and Medicinal Chemistry, Gifu Pharmaceutical University, Gifu, Japan

Key words

Adsorption, DNA damage, iron, mesothelial cell, multi-wall carbon nanotube

Correspondence

Shinya Toyokuni, Department of Pathology and Biological Responses, Nagoya University Graduate School of Medicine, 65 Tsurumai-cho, Showa-ku, Nagoya, Aichi 466-8550, Japan.
Tel: +81 52 744 2086; Fax: +81 52 744 2091;
E-mail: toyokuni@med.nagoya-u.ac.jp

Funding Information

Grant-in-aid for research from the Ministry of Education, Culture, Sports, Science and Technology (MEXT) of Japan (grant/award number: '24390094; 221S0001-04; 24108008'), the Yasuda Medical Foundation, National Cancer Center Research and Development Fund (grant/award number: '25-A-5').

Received October 5, 2015; Revised December 5, 2015; Accepted December 14, 2015

Cancer Sci **107** (2016) 250–257

doi: 10.1111/cas.12865

Multi-wall carbon nanotubes (MWCNT) are a form of flexible fibrous nanomaterial with high electrical and thermal conductivity. However, 50-nm MWCNT in diameter causes malignant mesothelioma (MM) in rodents and, thus, the International Agency of Research on Cancer has designated them as a possible human carcinogen. Little is known about the molecular mechanism through which MWCNT causes MM. To elucidate the carcinogenic mechanisms of MWCNT in mesothelial cells, we used a variety of lysates to comprehensively identify proteins specifically adsorbed on pristine MWCNT of different diameters (50 nm, NT50; 100 nm, NT100; 150 nm, NT150; and 15 nm/tangled, NTtngl) using mass spectrometry. We identified >400 proteins, which included hemoglobin, histone, transferrin and various proteins associated with oxidative stress, among which we selected hemoglobin and transferrin for coating MWCNT to further evaluate cytotoxicity, wound healing, intracellular catalytic ferrous iron and oxidative stress in rat peritoneal mesothelial cells (RPMC). Cytotoxicity to RPMC was observed with pristine NT50 but not with NTtngl. Coating NT50 with hemoglobin or transferrin significantly aggravated cytotoxicity to RPMC, with an increase in cellular catalytic ferrous iron and DNA damage also observed. Knockdown of transferrin receptor with ferristatin II decreased not only NT50 uptake but also cellular catalytic ferrous iron. Our results suggest that adsorption of hemoglobin and transferrin on the surface of NT50 play a role in causing mesothelial iron overload, contributing to oxidative damage and possibly subsequent carcinogenesis in mesothelial cells. Uptake of NT50 at least partially depends on transferrin receptor 1. Modifications of NT50 surface may decrease this human risk.

Carbon nanotubes (CNT) are a promising material in nanotechnologies due to their high thermal and mechanical resistance but high electrical and thermal conductivity, flexibility and semiconductivity.[1] Thus, CNT are used worldwide in various industrial and mechanical applications; they are used as components in electronics, energy-storage devices, solar cells and sensors, and as fillers in polymeric composites and concrete.[2,3] CNT have also been proposed for use in medicine as nanovectors or as substrates in tissue engineering.[4,5]

Asbestos fibers are naturally occurring hydrated silicates. Exposure to asbestos may induce various pathologies in humans, including pleural effusion, pleural plaques and pulmonary asbestosis. Furthermore, this material may cause malignant mesothelioma (MM) and/or lung cancer after a long incubation period.[6] Many rodent experiments support the carcinogenicity of asbestos, especially to mesothelial cells.[7–12] By 2006, at least 40 countries had banned or severely restricted asbestos use.[13] Having a diameter less than 200 nm and a length measured in μm, CNT have a needle-like shape with a high aspect ratio, which is similar to asbestos. Accordingly, there has been discussion that CNT might have similar carcinogenic properties to asbestos. Recently, three independent rodent studies revealed that 50-nm diameter multi-wall carbon nanotubes (MWCNT) cause MM when injected intraperitoneally to $p53^{+/-}$ knockout mice[14] or to wild-type rats[15] or intrascrotally to Fischer-344 rats.[16] In 2014, the International Agency of Research designated MWCNT 50 nm in diameter as a possible human carcinogen (Group 2B), based on these studies.[17] Of note, tangled CNT 15 nm in diameter induce no MM[18] and CNT, 150 nm are less carcinogenic, which may be partially associated with their difficulty in entering mesothelial cells.[15]

Here, we followed our previous strategy for asbestos-induced mesothelial carcinogenesis, which is similar to immunoprecipitation,[19,20] to elucidate the major molecular mechanisms of MWCNT-induced mesothelial carcinogenesis. We used mass spectrometry (MS) to exhaustively identify the proteins that adsorb on the surface of four pristine MWCNT of different diameters. Among these, we focused on hemoglobin and transferrin, both of which are associated with iron metabolism.

Materials and Methods

Materials and antibodies. Four types of vapor-grown MWCNT were obtained from Showa Denko (Tokyo, Japan). Characterization of the MWCNT is summarized in Table S1, based on our previous results.[15] Trypsin gold for MS was obtained from Promega (Madison, WI, USA). Albumin from bovine serum (BSA), human holo-transferrin and chlorazol black (ferristatin II)[21] were purchased from Sigma-Aldrich (St. Louis, MO, USA). The Silver Quest staining kit came from Invitrogen (Carlsbad, CA, USA). Antibodies against transferrin (ab1223), transferrin receptor 1 (ab84036), hemoglobin subunit α (ab92492) and peroxiredoxin 6 (ab59543) were purchased from Abcam (Cambridge, MA, USA); Keap1 (D6B12), histone H3 (D1H2), histone H2A (#2578) and histone H2B (#2722) from Cell Signaling Technology (Danvers, MA, USA); hemoglobin β (SC-31116) from Santa Cruz Biotechnology (Dallas, TX, USA); and 4-hydroxy-2-nonenal-modified proteins (HNEJ-2) from Nikken Seil (Fukuroi, Shizuoka, Japan).[22]

Preparation of tissue lysate. Lung, heart, liver and spleen from eight 24-week-old specific pathogen-free male or female Fischer-344 rats (SLC Japan, Hamamatsu, Japan) were homogenized at 4°C with lysis buffer (20 mM Tris-HCl, pH 7.4, 0.1% SDS) in the presence of protease inhibitors (cOmplete Mini; Roche, Basel, Switzerland), followed by sonication at 4°C for 30 s. After centrifugation (15 000 *g*) at 4°C for 10 min, the protein concentration was measured with a Protein Assay Bicinchninate Kit (Nacalai Tesque, Kyoto, Japan). The animal experiment committee of Nagoya University Graduate School of Medicine approved this experiment.

Preparation of multi-wall carbon nanotubes suspension and hemoglobin-coated or holo-transferrin-coated multi-wall carbon nanotubes. Multi-wall carbon nanotubes were suspended in 10 mM PBS, pH 7.4 (D-PBS[-]; Wako, Osaka, Japan) containing 0.5% BSA, and then sonicated at 4°C for 2 h to 5 mg/mL. As preparation of hemoglobin-coated or holo-transferrin-coated MWCNT, an amount of 400 μg of hemoglobin or holo-transferrin protein was added to 20 μL of 5 mg/mL MWCNT suspension. PBS containing 0.5% BSA was added up to 1 mL, followed by 3 h-incubation at 37°C. The mixture was centrifuged at 20 000 *g* for 2 min, and the supernatant was discarded. The pellet was washed three times with PBS containing 0.5% BSA. All samples were prepared immediately before use.

Protein adsorption on multi-wall carbon nanotubes. Immunoprecipitation-like assay (CNT immunoprecipitation) was performed as described.[19,20] Briefly, lysate (400 μg) and MWCNT (250 μg) were mixed, and PBS was added up to 1 mL. Crocidolite (UICC, Geneva, Switzerland) was used as a positive control. After 3-h incubation at 37°C, the mixture was centrifuged (15 000 *g*) at 4°C for 10 min. The pellets were washed five times with PBS. SDS-PAGE sample buffer was added, and the samples were boiled for 10 min. The samples were then centrifuged (15 000 *g*) at 4°C for 5 min, and the supernatants were evaluated with SDS-PAGE. The gel was stained with a silver staining kit.

Assessment of multi-wall carbon nanotube adsorption ability. To calculate the amount of proteins adsorbed on the surfaces of the MWCNT, the concentration of proteins remaining in the supernatant was measured using a spectrophotometer (NanoDrop 2000; Thermo Fisher Scientific, Waltham, MA, USA), which was deducted from the control value.

Identification of proteins adsorbed on multi-wall carbon nanotube with liquid chromatography/mass spectrometry/mass spectrometry. Mass spectrometric identification of the proteins was performed as described previously.[19,23] Briefly, for in-gel digestion, proteins run on SDS-PAGE were visualized with silver staining; each band was excised from the gels and subjected to in-gel digestion with trypsin in a buffer containing 25 mM ammonium bicarbonate overnight at 37°C. For in-solution digestion, the proteins were detached from MWCNT by degeneration with guanidinium chloride and digested with trypsin in the same manner. Molecular mass analysis of the tryptic peptides was performed with an LTQ Orbitrap XL (Thermo Fisher Scientific). Proteins were identified by liquid chromatography/mass spectrometry/mass spectrometry, and theoretical peptide masses from the proteins were registered in Swiss-Prot. The experiments were performed in triplicate.

Western blotting. This was performed as previously described.[24]

Cell culture. Rat peritoneal mesothelial cells (RPMC) were produced as described,[25,26] plated at a density of 3×10^4 cells/cm^2 and incubated for 24 h. RPMC were cultured in RPMI-1640 medium (189-02025; Wako) with 10% FBS (Biowest, Nuaillé, France) and 1% Antibiotic–Antimycotic (15240-062; Invitrogen). RPMC were maintained in a humidified incubator at 37°C with 5% CO_2, as described previously.[27]

Multi-wall carbon nanotube cytotoxicity assay. RPMC were plated at a density of 3×10^4 cells/cm^2 and incubated for 24 h before adding MWCNT. MWCNT were added to RPMC to a final concentration of 10 μg/cm^2. After 72-h incubation, dead-cell protease activity assay (CytoTox-Glo Cytotoxicity Assay; Promega) was used to measure the cytotoxicity.

Wound-healing assay. RPMC were plated at a density of 3×10^4 cells/cm^2 and incubated to confluence. RPMC were given a straight scratch with a pipette, followed by washing three times with PBS. MWCNT were added to RPMC at a final concentration of 10 μg/cm^2. The same procedure, without adding the MWCNT, was performed as a control. Pictures were taken 0, 8 and 24 h later with the optical microscope. The wounded area was evaluated with ImageJ (imagej.nih.gov/ij/; NIH, Bethesda, MD, USA).

Visualization of intracellular catalytic ferrous ion (Fe[II]). RhoNox-1 (10 μM, 30-min incubation at 37°C) was used as described.[28,29] RPMC were plated at a density of 3×10^4 cells/cm^2 and incubated for 24 h before adding MWCNT to a final concentration of 10 μg/cm^2. As a control, medium was added. After 24-h incubation, the cells were stained and observed with a fluorescent microscope (BZ-9000; Keyence Corporation; Osaka, Japan).

Lipid peroxidation assay. We evaluated lipid peroxidation, using an antibody against 4-hydroxy-2-nonenal (HNE) and BODIPY (581/591) C_{11} as the lipid peroxidation sensor probe (Thermo Fisher). RPMC were plated at a density of 3×10^4 cells/cm^2 and incubated for 24 h before adding MWCNT to a final concentration of 10 μg/cm^2. For western blot analysis, after treating cells with MWCNT for 24 h, the cells were collected and lysed with lysis buffer. For BODIPY (581/591) C_{11}, after treating cells with MWCNT for 24 h, BODIPY C_{11} (final concentration 5 μM) was added to 5×10^6 cells per mL, incubated for 15 min at room temperature and washed twice (200 *g* for 5 min), which was analyzed with a Gallios flow cytometer (Beckman Coulter, Brea, CA, USA).

Comet assay. Alkaline comet assay was performed according to the method of Dhawan *et al.*[30] with modifications. Approx-

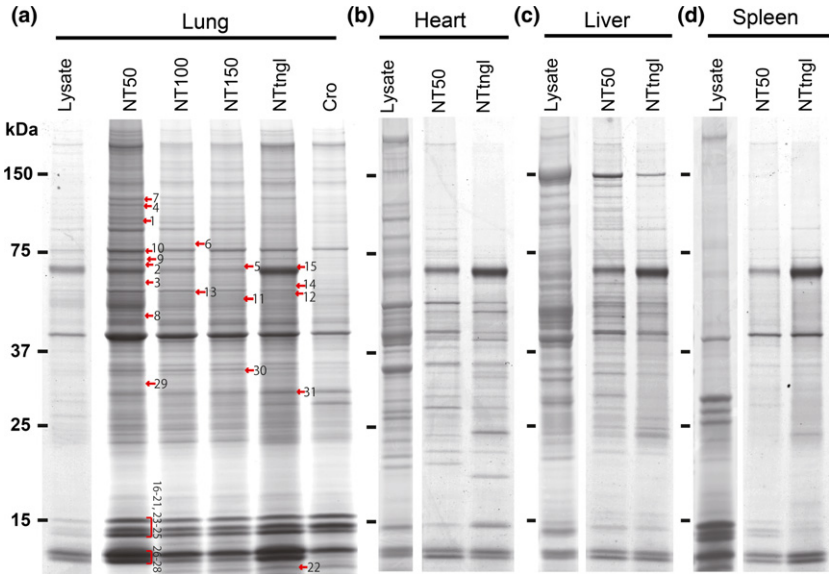

Fig. 1. Adsorption of specific proteins on multi-wall carbon nanotubes (MWCNT). Lysates from (a) lung, (b) heart, (c) liver or (d) spleen were incubated with MWCNT of four distinct diameters (NT50, NT100, NT150 and NTtngl; 50, 100, 150 and 15 nm [tangled], respectively), washed and analyzed by SDS-PAGE followed by silver staining. The original band patterns of the lysates are shown for comparison. Notably, each MWCNT showed specific adsorption. NT50 revealed the highest protein adsorption with a higher number of protein bands. The numbers with red arrows correspond to those in Table 2, in which the in-gel digestion method was used for protein identification. Please refer to the text for details. Cro, crocidolite.

Table 1. A summarized result of in-solution digestion method

Accession	Mass	Original lysate	Biological role
VIME_RAT	53 700	1, 2, 3, 4	Vimentin
ALBU_RAT	68 686	1, 3, 4	Serum albumin
ATPB_RAT	56 318	1, 3, 4	ATP synthase subunit beta, mitochondrial
TRFE_RAT	76 346	1, 2, 3, 4	Serotransferrin
MOES_RAT	67 697	1, 2, 3, 4	Moesin
ACTB_RAT	41 710	1, 2, 3, 4	Actin, cytoplasmic 1
K1C19_RAT	44 609	1, 2, 3, 4	Keratin, type I cytoskeletal 19
A1I3_RAT	163 670	1, 3, 4	Alpha-1-inhibitor 3
DESM_RAT	53 424	1, 2, 3, 4	Desmin
EHD2_RAT	61 199	1, 2, 3, 4	EH domain-containing protein 2
ATPA_RAT	59 717	1, 2, 3, 4	ATP synthase subunit alpha, mitochondrial
ACTA_RAT	41 982	1, 2, 3, 4	Actin, aortic smooth muscle
HSP7C_RAT	70 827	1, 2, 3, 4	Heat shock cognate 71 kDa protein
LMNA_RAT	74 279	1, 2, 3, 4	Prelamin-A/C
ACTC_RAT	41 992	1, 3, 4	Actin, alpha cardiac muscle 1
MUG1_RAT	165 221	4	Murinoglobulin-1
HBB1_RAT	15 969	1, 2, 3, 4	Hemoglobin subunit beta-1
TBB4B_RAT	49 769	1, 2, 3, 4	Tubulin beta-4B chain
K2C8_RAT	53 985	1, 2, 3, 4	Keratin, type II cytoskeletal 8
SPTN1_RAT	284 462	1, 4	Spectrin alpha chain, non-erythrocytic 1
TBA1B_RAT	50 120	1, 2, 3, 4	Tubulin alpha-1B chain
ENOA_RAT	47 098	1, 2, 3, 4	Alpha-enolase
TBA1A_RAT	50 104	1, 2, 3, 4	Tubulin alpha-1A chain
HBB2_RAT	15 972	1, 2, 3, 4	Hemoglobin subunit beta-2
K1C10_RAT	56 470	1, 2, 3, 4	Keratin, type I cytoskeletal 10
PTRF_RAT	43 882	1, 2, 3, 4	Polymerase I and transcript release factor
TBB2A_RAT	49 875	1	Tubulin beta-2A chain
DPYL2_RAT	62 239	1, 2, 3, 4	Dihydropyrimidinase-related protein 2
TBB5_RAT	49 639	1, 2, 3, 4	Tubulin beta-5 chain
MYH9_RAT	226 197	1, 2, 3, 4	Myosin-9

1, NT50; 2, NT100; 3, NT150; 4, NTtngl. Refer to Table S2 for details.

Table 2. A summarized result of in-gel digestion method

Band number	Accession	Mass	Protein name
1	IQCAL_RAT	95 625	IQ and AAA domain-containing protein 1-like
2	KEAP1_RAT	69 399	Kelch-like ECH-associated protein 1
3	CP270_RAT	56 157	Cytochrome P450 2C70
4	MCM9_RAT	124 125	DNA helicase MCM9
5	DCAF8_RAT	66 156	DDB1- and CUL4-associated factor 8
6	SO4C1_RAT	78 648	Solute carrier organic anion transporter family member 4C1
7	NOS2_RAT	130 628	Nitric oxide synthase, inducible
8	ACTB_RAT	41 737	Actin, cytoplasmic 1
9	MOES_RAT	67 739	Moesin
10	TRFE_RAT	76 395	Serotransferrin
11	GBRP_RAT	50 481	Gamma-aminobutyric acid receptor subunit pi
12	SBP1_RAT	52 532	Selenium-binding protein 1
13	AL1A1_RAT	54 459	Retinal dehydrogenase 1
14	ALDH2_RAT	56 488	Aldehyde dehydrogenase, mitochondrial
15	FETA_RAT	68 386	Alpha-fetoprotein
16	H2A1C_RAT	14 105	Histone H2A type 1-C
17	H2A1F_RAT	14 176	Histone H2A type 1-F
18	H2AJ_RAT	14 045	Histone H2A.J
19	H2B1_RAT	13 990	Histone H2B type 1
20	H2B1A_RAT	14 225	Histone H2B type 1-A
21	H31_RAT	15 404	Histone H3.1
22	H4_RAT	11 367	Histone H4
23	RL23_RAT	14 865	60S ribosomal protein L23
24	RS16_RAT	16 445	40S ribosomal protein S16
25	RS14_RAT	16 259	40S ribosomal protein S14
26	HBA_RAT	15 329	Hemoglobin subunit alpha-1/2
27	HBB1_RAT	15 979	Hemoglobin subunit beta-1
28	HBB2_RAT	15 982	Hemoglobin subunit beta-2
29	ROA1_RAT	34 212	Heterogeneous nuclear ribonucleoprotein A1
30	ROA2_RAT	37 478	Heterogeneous nuclear ribonucleoproteins A2/B1
31	CAH2_RAT	29 114	Carbonic anhydrase 2

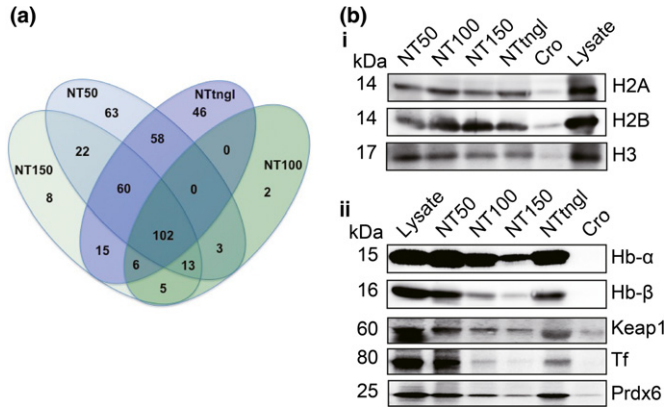

Fig. 2. Analysis of adsorbed proteins identified with mass spectrometry. Proteins adsorbed on the surface of each multi-wall carbon nanotubes (MWCNT) were identified with liquid chromatography/mass spectrometry/mass spectrometry (LC/MS/MS). The results from each sample were compared for overlap (a). Three histones (H2A, H2B and H3), two subunits of hemoglobin (Hb-α and Hb-β) and three other proteins (Tf, transferrin; Prdx6, peroxiredoxin 6; Keap1, Kelch-like ECH-associated protein 1) associated with oxidative stress and based on our previous experiments on asbestos were picked from the common cluster and were confirmed with western blotting analysis (b). Please refer to the text for details.

imately 8000 cells in 10 μL or less volume were mixed with 50 μL of low melting point agarose and layered on the CometSlide (CommetAssay; Trevigen, Gaithersburg, MD, USA). After preparation, the slide was immersed in lysis solution and refrigerated at 4°C for 2 h. After lysis, the slide was placed in alkaline electrophoresis buffer for 30 min to allow salt equilibration and further DNA unwinding. Electrophoresis was performed at 300 mA for 30 min at 4°C. The slide was then washed three times with neutralization buffer for 10 min. The cells were stained with 50 μL of ethidium bromide. Comet images were taken with a fluorescent microscope. The tail moment of the DNA was analyzed using an image analysis system (casplab.com),[31] and the tail length was scored by direct measurement. A total of 50 cells were analyzed per sample for quantitation.

Apoptosis assay. TACS Annexin V Kit (Trevigen) was used according to the protocol provided in the kits. The stained cells were analyzed using a Gallios flow cytometer.

Ferristatin II treatment to downregulate the transferrin receptor. RPMC were plated at a density of 3×10^4 cells/cm^2. After 24 h of incubation, cells were washed three times with PBS containing 1 mM $MgCl_2$ and 0.1 mM $CaCl_2$ (PBS++) and then washed once with serum-free medium. After adding 50 μM ferristatin II or dimethyl sulfoxide as a vehicle control to the RPMC in serum-free medium, the cells were incubated at 37°C with 5% CO_2 for 4 h, as described previously.[21]

Measurements of multi-wall carbon nanotubes in cells. We added MWCNT to the ferristatin II-treated or non-treated RPMC at a concentration of 10 μg/cm^2. After 24 h of incubation, the amounts of MWCNT taken up by cells were calculated by flow cytometry, as described previously.[32,33]

Statistical analysis. A two-way ANOVA, a one-way ANOVA or an unpaired Student's *t*-test was applied. $P < 0.05$ was considered statistically significant.

Results

Proteins adsorbed on the surface of multi-wall carbon nanotubes. We named the MWCNT NT50, NT100, NT150 and NTtngl, according to their average diameter, as described previously.[15] Figure 1 shows a variety of proteins after CNT precipitation and gel electrophoresis followed by silver staining. Regarding the lung lysate, the banding pattern of each CNT showed a similar pattern, including crocidolite. NT50

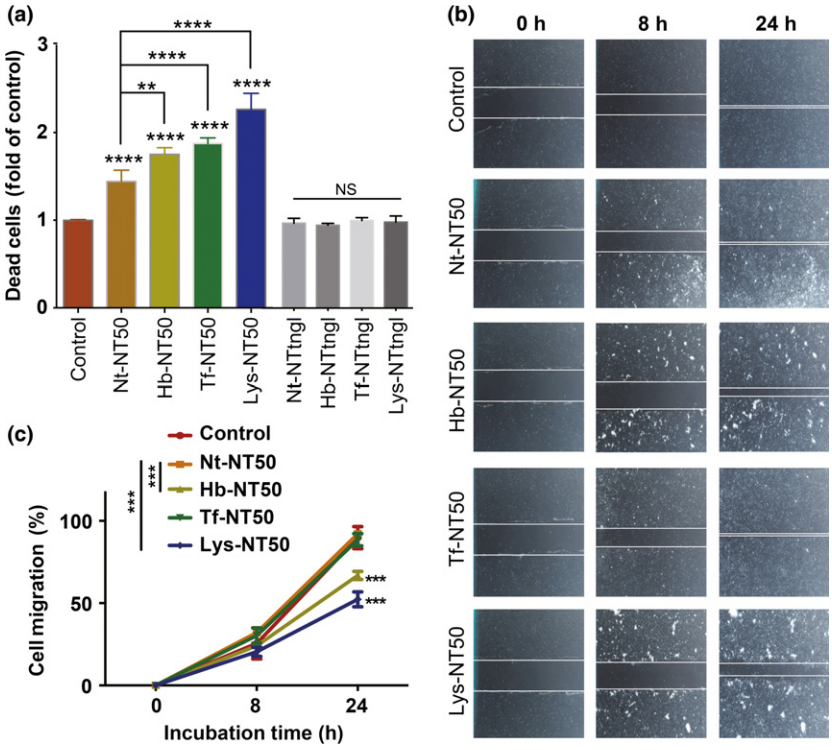

Fig. 3. Hemoglobin-coating or holo-transferrin-coating increases the cytotoxicity of multi-wall carbon nanotubes (MWCNT) to rat peritoneal mesothelial cells. A study of cell viability in rat peritoneal mesothelial cells after a 72-h incubation with protein-coated NT50 (coated with hemoglobin, Hb-NT50; coated with transferrin, Tf-NT50; coated with lung lysate, Lys-NT50) at 10 μg/cm^2 revealed higher cytotoxicity than pristine non-treated NT50 (Nt-NT50). This effect was not observed in NTtngl, even after the same coating procedures (a). Wound healing assays showed that hemoglobin or lung lysate coating retarded cellular proliferation compared to Nt-NT50 (b, c) ($N = 3$, means ± SEM; $^{**}P < 0.01$, $^{***}P < 0.005$, $^{****}P < 0.001$ *vs* control otherwise specified; NS, not significant).

revealed the highest adsorption with the highest number of protein bands (Fig. 1a). However, the banding patterns were different between NT50 and NTtngl when heart, liver and spleen were analyzed (Fig. 1b–d). Each protein's affinity to each CNT was distinct.

Identification of proteins with mass spectrometry. To exhaustively identify proteins adsorbed on MWCNT, we undertook both in-solution and in-gel digestion methods. With the in-solution digestion method, we identified 321 proteins from NT50, 131 proteins from NT100, 231 proteins from NT150 and 287 proteins from NTtngl (Tables 1 and S2). The results of the in-solution digestion method revealed that NT50 and NTtngl shared the highest number of proteins among the four MWCNT (Fig. 2a). More than 400 proteins were identified and classified (Table S2). These included histones and many proteins associated with iron metabolism or oxidative stress. We picked up histones 2A/2B/3, hemoglobin α chain, hemoglobin β chain, Keap1, transferrin and peroxiredoxin 6 for confirmation (Fig. 2b). For histones, each of the four CNT fiber types revealed similar affinities (Fig. 2b[i]). However, for the other proteins studied, NT50 and NTtngl adsorbed significantly larger amounts of the proteins investigated than did NT100, NT150 or crocidolite, with similar affinities, except for transferrin (Fig. 2b[ii]). Generally, the results were proportional to the surface area of each CNT (Fig. S1). NT50, which is potently carcinogenic to mesothelial cells, showed a higher affinity for transferrin than NTtngl, which shows no carcinogenicity to mesothelial cells.[18]

Protein coating increased the cytotoxicity of multi-wall carbon nanotubes. We evaluated the cytotoxicity of MWCNT to RPMC with a dead-cell protease activity assay (Fig. 3a). The RPMC were exposed to pristine CNT (Nt-NT50) or CNT after incubation with hemoglobin (Hb-NT50), holo-transferrin (Tf-NT50) or lung lysate (Lys-NT50). NT50 and NTtngl were used as carcinogenic and non-carcinogenic CNT, respectively. The cells treated with Nt (non-treated)-NT50 showed approximately 1.4-fold dead cells, and Hb-NT50 and Tf-NT50 revealed approximately 1.8-fold and 1.9-fold dead cells, respectively, compared with the untreated control. Lys-NT50 induced the most dead cells with an approximate 2.3-fold increase. In contrast, neither pristine NTtngl (Nt-NTtngl) nor NTtngl after incubation with Hb (Hb-NTtngl) or Tf (Tf-NTtngl) showed cytotoxicity to RPMC. We also performed a wound-healing assay to evaluate the proliferation of RPMC (Fig. 3b,c). Nt-NT50 and Tf-NT50 decreased the proliferation of cells by approximately 10%. However, Hb-NT50 and Lys-NT50 caused 24% and 31% decreases, respectively.

Hemoglobin-coated or holo-transferrin-coated NT50 increased intracellular catalytic Fe(II) in association with lipid peroxidation. RhoNox-1 was used to visualize catalytic (labile) Fe(II). We confirmed that neither hemoglobin nor holo-transferrin increase the fluorescence intensity of RhoNox-1 (Fig. S2). After treatment with Hb-NT50 or Tf-NT50, catalytic Fe(II) in cells increased more significantly than in the cells treated with Nt-NT50 (Fig. 4a). In contrast, neither Hb-NTtngl, Tf-NTtngl nor Nt-NTtngl affected the intracellular catalytic Fe(II). To assess whether increased catalytic Fe(II) induces oxidative stress in cells, lipid peroxidation products, 4-hydroxy-2-nonenal (HNE)-modified proteins,[22] were measured as a marker of oxidative stress by western blot with a monoclonal antibody

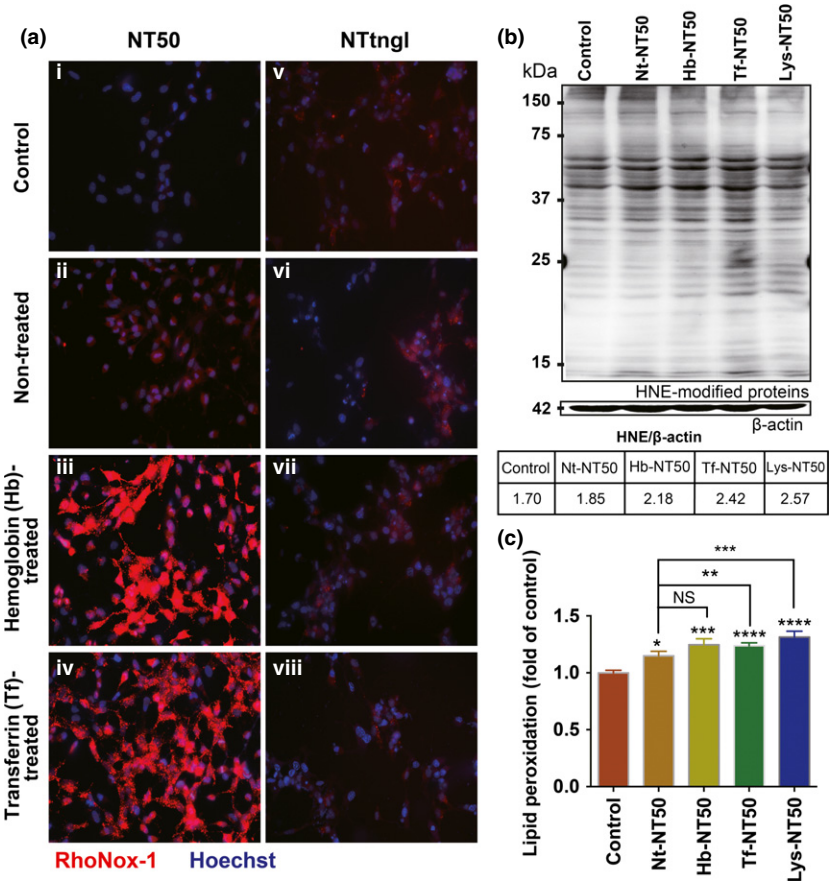

Fig. 4. Take-up of hemoglobin-coated or transferrin-coated NT50 by rat peritoneal mesothelial cells increases the intracellular catalytic Fe(II). After incubating rat peritoneal mesothelial cells with hemoglobin-coated or transferrin-coated NT50 (i–iv) or NTtngl with the same coatings (v–viii), the cells were stained with a fluorescent probe (Rhonox-1) that is highly specific to catalytic Fe(II) (a). Intracellular catalytic Fe(II) was significantly increased only in the case of hemoglobin-coated or transferrin-coated NT50, but not NTtngl. The levels of lipid peroxidation were evaluated with an antibody against 4-hydroxy-2-nonenal (HNE)-modified proteins (b), and lipid peroxidation sensor probe BODIPY (581/591) C_{11} (c), which were consistent with the amounts of catalytic Fe(II) ($N = 3$, means ± SEM; $^{*}P < 0.05$, $^{**}P < 0.01$, $^{***}P < 0.005$, $^{****}P < 0.001$ *vs* control otherwise specified).

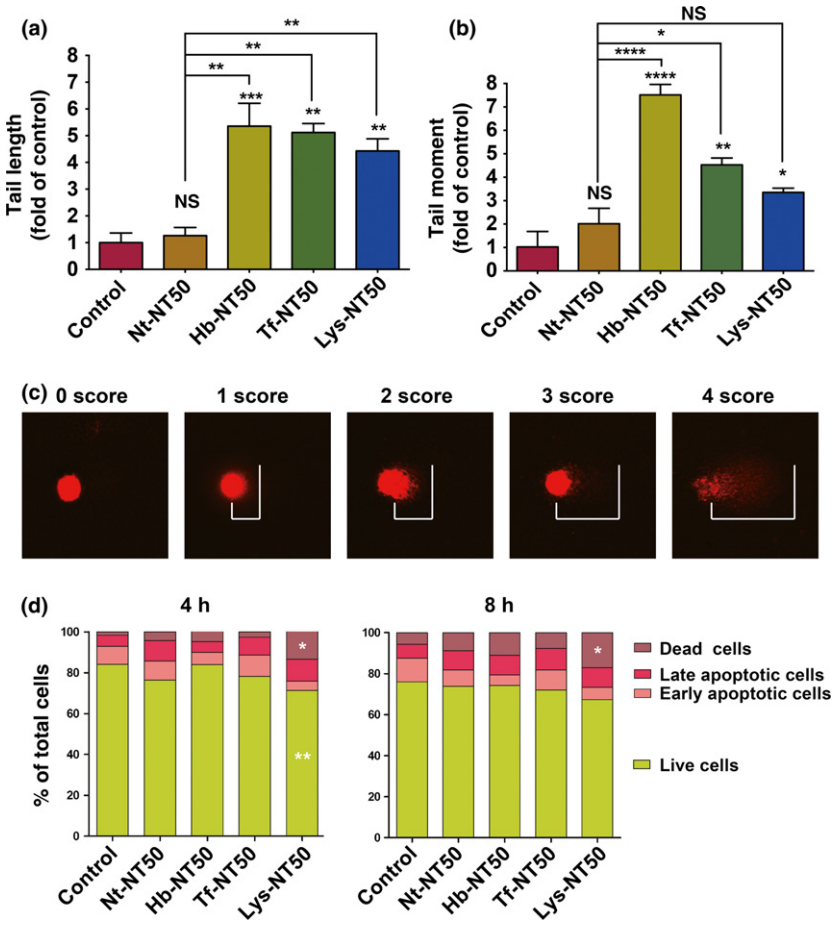

Fig. 5. Hemoglobin-coating or holo-transferrin-coating of multi-wall carbon nanotubes (MWCNT) induces DNA damage to rat peritoneal mesothelial cells without causing apoptosis. We used a comet assay to determine whether protein coating may cause DNA damage in rat peritoneal mesothelial cells. Tail length (a). Tail moment (b). Examples of scoring in comet assay (c). We observed a significant increase in dead cells, presumably through apoptosis, only when lung lysate was used to coat NT50 after 4 or 8 h of incubation (d; N=3, means ± SEM; $*P < 0.05$, $**P < 0.01$, $***P < 0.005$, $****P < 0.001$ *vs* control otherwise specified; NS, not significant).

(Fig. 4b), and flow cytometry was used with a lipid peroxidation sensor probe BODIPY (581/591) C_{11} (Fig. 4c). Treatment with Nt-NT50 significantly increased lipid peroxidation, which was aggravated with the use of Tf-NT50 or Lys-NT50.

Hemoglobin-treated or holo-transferrin-treated NT50 increased DNA damage. We used RPMC exposed to hemoglobin-treated or holo-transferrin-treated NT50 for comet assay. Two measures, tail length (length of DNA fragment) and tail moment (amount of DNA fragment in tail), were used to evaluate the DNA damage. Whereas no significant increase in tail length or tail moment was observed with Nt-NT50, coating with Hb, Tf or lung lysate significantly increased these measures (Fig. 5a–c). Notably, we observed an increase in dead cells, presumably via apoptosis, only in Lys-NT50 (Fig. 5d).

Transferrin receptor plays a role in the uptake of Tf-NT50. After treating RPMC with Nt-NT50 or Lys-NT50, we observed a difference in uptake, suggesting that an interaction between nanotube surface protein and its receptor may promote NT50

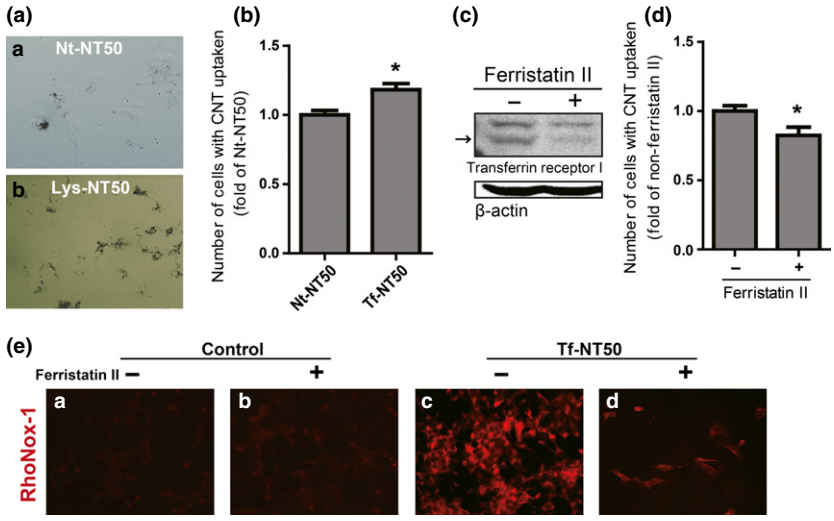

Fig. 6. Transferrin receptor 1 plays a role in the uptake of NT50 by rat peritoneal mesothelial cells. Difference in the uptake of NT50 by rat peritoneal mesothelial cells with ([b] Lys-NT50) or without ([a] Nt-NT50) protein coating (a). The number of cells which internalized or attached Nt-NT50 or Tf-NT50 was measured by flow cytometer (b). Ferristatin II reduced the levels of transferrin receptor 1 (arrow) (c), which induced decreased uptake of Tf-NT50 (d). Whereas ferristatin II treatment alone did not change the level of cytoplasmic catalytic Fe(II), ferristatin II treatment significantly decreased the amounts of catalytic Fe(II) upon exposure to Tf-NT50 ($N = 3$, means ± SEM). Please refer to the text and Figure 4 for details. CNT, carbon nanotubes.

internalization (Fig. 6a). To evaluate whether NT50 uptake was associated with the plasma membrane receptor for Tf, flow cytometric analysis was performed[33] to calculate the number of cells revealing NT50 uptake by counting 10 000 cells. Tf-NT50 induced approximately 20% more uptake of CNT by RPMC than Nt-NT50 (Fig. 6b). TfR1 (TFRC, CD71) is the main receptor of transferrin. Ferristatin II is a specific inhibitor of TfR1, and the ferristatin II-induced decrease in TfR1 protein levels was confirmed with western blot analysis (Fig. 6c). Ferristatin II significantly decreased the amount of Tf-NT50 penetrating the cells (Fig. 6d). Simultaneously, the level of catalytic ferrous iron was also decreased in Tf-NT50-treated cells after ferristatin II addition (Fig. 6e).

Discussion

Risk assessment of CNT is important because CNT are already in the market due to their superb utility as an industrial material.[2,3] We previously observed that carcinogenic NT50 was likely to enter mesothelial cells, probably via penetration.[15,34] Based on our previous asbestos studies, we used lysates from various rat organs including lung, which is a putative major target for exposure in humans. Here we identified >400 proteins adsorbed on these CNT (Tables 1 and S2). The 104 adsorptive proteins, common to all four of the MWCNT tested, included hemoglobin (Hb), transferrin (Tf), histones, DNA helicase, actin and tubulin. Of note, asbestos did not adsorb Tf in our previous experiments,[19] but all of the other proteins above were in common with asbestos. Many proteins were associated with oxidative stress in the current experiments on MWCNT, which included Keap1, cytochrome P450, aldehyde dehydrogenase, thioredoxin, glutathione *S*-transferase, heat shock protein, peroxiredoxin and proteasome (Table S2).

Among those proteins, we decided to focus on Hb and Tf, considering not only the result that only CNT, especially NT50, adsorbed Tf but also a close association between excess iron and carcinogenesis.[35] Approximately 60% of the iron in humans is present in the heme of Hb in erythrocytes. Due to its richness in capillaries, lung tissue contains a large amount of Hb.

Coating NT50 with Hb or Tf significantly increased mesothelial damage (Fig. 3a) and significantly delayed wound healing with Hb or lung lysate (Fig. 3b,c); a similar effect was not observed with NTtngl, likely because NTtngl does not enter mesothelial cells.[15] We evaluated the effects of NT50 coated with Hb and Tf from the viewpoint of catalytic Fe(II) and lipid peroxidation. Catalytic Fe(II) can initiate the Fenton reaction that generates hydroxyl radicals to start lipid peroxidation.[36,37] Hb and Tf coating significantly increased the catalytic Fe(II) in RPMC detected with RhoNox-1[29] and HNE-modified proteins[38] simultaneously (Fig. 4), suggesting that NT50 exposure induces high levels of oxidative stress in mesothelial cells. This was also supported by an observation of increased intracellular Tf itself with western blot analysis (data not shown).

Then, we evaluated whether oxidative stress can cause DNA damage with the comet assay and found that only Hb-coated or Tf-coated NT50 induced DNA strand breaks in mesothelial cells, whereas pristine NT50 did not (Fig. 5a,b). Mesothelial damage with less cellular death in the case of Hb or Tf coating (Fig. 5d) might contribute to more mutations in mesothelial cells through NT50. We interpret here that Hb-coated or Tf-coated NT50 can induce various kinds of DNA damage, including DNA double-strand breaks. Thus, further studies are necessary to identify and quantify precise DNA lesions.

In the previous carcinogenesis experiments, we observed iron accumulation in areas near CNT deposits.[15] Excess iron has been associated with DNA strand breaks,[39,40] which may lead to homozygous deletion of *Cdkn2A/2B*, as observed in Fenton reaction-induced renal carcinogenesis in rats.[41,42] Reportedly, iron overload is a major pathogenesis in asbestos-induced mesothelial carcinogenesis, including the case of chrysotile containing no iron *per se*, where hemolysis followed by surface Hb adsorption induces similar pathology of iron overload.[11] Together with our previous finding of a high incidence of homozygous deletion of *Cdkn2A/2B* in CNT-induced mesothelial carcinogenesis,[15] these new results strongly support the hypothesis that excess iron possibly derived from Hb and Tf plays a role in the molecular mechanism of NT50-induced mesothelial carcinogenesis.

Finally, we evaluated the role of Tf receptor 1, based on the result that coating NT50 with lung lysate or Tf significantly increased the uptake of NT50 by RPMC (Fig. 6a,b). Decreasing Tf receptor 1 with ferristatin II significantly decreased NT50 uptake and cytoplasmic catalytic Fe(II) (Fig. 6c–e). These findings demonstrate, for the first time, the involvement of Tf and its receptor in the NT50 uptake by mesothelial cells, in addition to simple penetration, which provided a new molecular mechanism of MWCNT in mesothelial cell damage. Surprisingly, 18% decrease in the uptake of NT50 dramatically changed intracellular catalytic Fe(II). This may be associated with iron metabolism in mesothelial cells, especially storage and export, which needs further investigation.

In conclusion, our results suggest that adsorptive activity of NT50 for proteins, especially hemoglobin and transferrin, is a major mechanism in mesothelial damage followed by carcinogenesis. It works for the efficient NT50 uptake by mesothelial cells and also for the increased catalytic Fe(II), leading to DNA damage (Fig. 7). Therefore, chemical modification of CNT to avoid Hb and Tf adsorption might decrease the human risk to CNT-induced mesothelial carcinogenesis. Many more adsorptive proteins on MWCNT await evaluation.

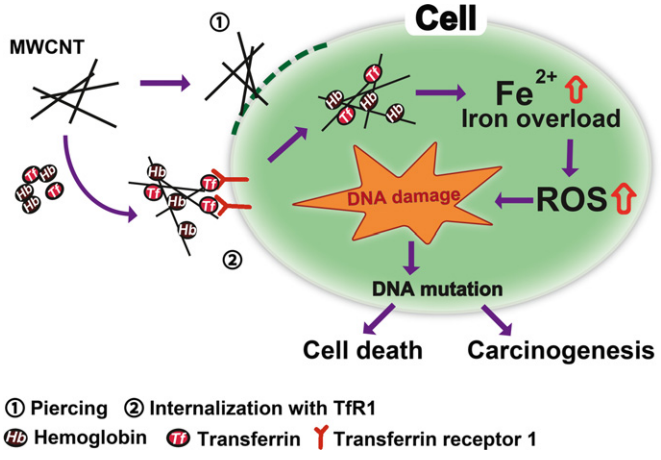

Fig. 7. Role of hemoglobin and transferrin in multi-wall carbon nanotube (MWCNT)-induced mesothelial injury and carcinogenesis. Adsorption of hemoglobin and transferrin on MWCNT provides another molecular mechanism to injure mesothelial cells, which is distinct from direct physical injury such as piercing.

Acknowledgments

This work was supported, in part, by the National Cancer Center Research and Development Fund (25-A-5), a Grant-in-aid for research

from the Ministry of Education, Culture, Sports, Science and Technology (MEXT) of Japan (24390094; 221S0001-04; 24108008), the Yasuda Medical Foundation and National Cancer Center Research and Development Fund (25-A-5). The authors wish to thank Nobuaki Misawa for excellent technical assistance with the pathologic specimens.

Disclosure Statement

The authors have no conflict of interest to declare.

References

1 Iijima S. Helical microtubules of graphitic carbon. *Nature* 1991; **354**: 56–8.
2 Endo M, Strano MS, Ajayan PM. Potential applications of carbon nanotubes. In: Ado J, Dresselhaus G, Dresselhaus MS, eds. *Carbon Nanotubes*, 1st edn. Heidelberg: Springer, 2008; 13–62.
3 Lee J, Mahendra S, Alvarez PJJ. Nanomaterials in the construction industry: a review of their applications and environmental health and safety considerations. *ACS Nano* 2010; **4**: 3580–90.
4 Liu Z, Tabakman S, Welsher K, Dai H. Carbon nanotubes in biology and medicine: in vitro and in vivo detection, imaging and drug delivery. *Nano Res* 2009; **2**: 85–120.
5 Zhang Y, Bai Y, Yan B. Functionalized carbon nanotubes for potential medicinal applications. *Drug Discov Today* 2010; **15**: 428–35.
6 Kamp DW. Asbestos-induced lung diseases: an update. *Transl Res* 2009; **153**: 143–52.
7 Wagner J, Berry G, Skidmore J, Timbrell V. The effects of the inhalation of asbestos in rats. *Br J Cancer* 1974; **29**: 252–69.
8 Bolton R, Davis J, Donaldson K, Wright A. Variations in the carcinogenicity of mineral fibres. *Ann Occup Hyg* 1982; **26**: 569–82.
9 Whitaker D, Shilkin K, Walters M. Cytologic and tissue culture characteristics of asbestos-induced mesothelioma in rats. *Acta Cytol* 1984; **28**: 185–9.
10 Suzuki Y, Kohyama N. Malignant mesothelioma induced by asbestos and zeolite in the mouse peritoneal cavity. *Environ Res* 1984; **35**: 277–92.
11 Jiang L, Akatsuka S, Nagai H *et al.* Iron overload signature in chrysotile-induced malignant mesothelioma. *J Pathol* 2012; **228**: 366–77.
12 Aierken D, Okazaki Y, Chew SH *et al.* Rat model demostrates a high risk of tremolite but a low risk of anthophyllite for mesothelial carcinogenesis. *Nagoya J Med Sci* 2014; **76**: 149–60.
13 Wagner GR. The fallout from asbestos. *Lancet* 2007; **369**: 973–4.
14 Takagi A, Hirose A, Nishimura T *et al.* Induction of mesothelioma in p53+/− mouse by intraperitoneal application of multi-wall carbon nanotube. *J Toxicol Sci* 2008; **33**: 105–16.
15 Nagai H, Okazaki Y, Chew S *et al.* Diameter of multi-walled carbon nanotubes is a critical factor in mesothelial injury and subsequent carcinogenesis. *Proc Natl Acad Sci U S A* 2011; **108**: E1330–8.
16 Sakamoto Y, Nakae D, Fukumori N *et al.* Induction of mesothelioma by a single intrascrotal administration of multi-wall carbon nanotube in intact male Fischer 344 rats. *J Toxicol Sci* 2009; **34**: 65–76.
17 Grosse Y, Loomis D, Guyton KZ *et al.* Carcinogenicity of fluoro-edenite, silicon carbide fibres and whiskers, and carbon nanotubes. *Lancet Oncol* 2014; **15**: 1427–8.
18 Nagai H, Okazaki Y, Chew SH *et al.* Intraperitoneal administration of tangled multiwalled carbon nanotubes of 15 nm in diameter does not induce mesothelial carcinogenesis in rats. *Pathol Int* 2013; **63**: 457–62.
19 Nagai H, Ishihara T, Lee WH *et al.* Asbestos surface provides a niche for oxidative modification. *Cancer Sci* 2011; **102**: 2118–25.
20 Kubo Y, Takenaka H, Nagai H, Toyokuni S. Distinct affinity of nuclear proteins to the surface of chrysotile and crocidolite. *J Clin Biochem Nutr* 2012; **51**: 221–6.
21 Byrne SL, Buckett PD, Kim J *et al.* Ferristatin II promotes degradation of transferrin receptor-1 in vitro and in vivo. *PLoS One* 2013; **8**: e70199.
22 Toyokuni S, Miyake N, Hiai H *et al.* The monoclonal antibody specific for the 4-hydroxy-2-nonenal histidine adduct. *FEBS Lett* 1995; **359**: 189–91.
23 Yamashita K, Nagai H, Toyokuni S. Receptor role of annexin A2 in the mesothelial endocytosis of crocidolite fibers. *Lab Invest* 2015; **95**: 749–64.
24 Toyokuni S, Kawaguchi W, Akatsuka S, Hiroyasu M, Hiai H. Intermittent microwave irradiation facilitates antigen-antibody reaction in Western blot analysis. *Pathol Int* 2003; **53**: 259–61.
25 Yamashita Y, Tsurumi T, Mori N, Kiyono T. Immortalization of Epstein-Barr virus-negative human B lymphocytes with minimal chromosomal instability. *Pathol Int* 2006; **56**: 659–67.
26 Jiang L, Yamashita Y, Toyokuni S. A novel method for efficient collection of normal mesothelial cells *in vivo*. *J Clin Biochem Nutr* 2010; **46**: 265–8.
27 Jiang L, Yamashita Y, Chew SH *et al.* Connective tissue growth factor and β-catenin constitute an autocrine loop for activation in rat sarcomatoid mesothelioma. *J Pathol* 2014; **233**: 402–14.
28 Hirayama T, Okuda K, Nagasawa H. A highly selective turn-on fluorescent probe fro iron(II) to visualize labile iron in living cells. *Chem Sci* 2013; **4**: 1250–6.
29 Mukaide T, Hattori Y, Misawa N *et al.* Histological detection of catalytic ferrous iron with the selective turn-on fluorescent probe RhoNox-1 in a Fenton reaction-based rat renal carcinogenesis model. *Free Radic Res* 2014; **48**: 402–14.
30 Dhawan A, Bajpayee MM, Pandey AK, Parmar D. Protocol for the single cell gel electrophoresis/comet assay for rapid genotoxicity assessment. *Sigma* 2003; **1077**: 1.
31 Końca K, Lankoff A, Banasik A *et al.* A cross-platform public domain PC image-analysis program for the comet assay. *Mutat Res* 2003; **534**: 15–20.
32 Al-Jamal KT, Kostarelos K. Assessment of cellular uptake and cytotoxicity of carbon nanotubes using flow cytometry. In: Balasubramanian K, Burghard M, eds. *Carbon Nanotubes Methods and Protocols*, 1st edn. New York: Springer, 2010; 123–34.
33 Yamashita K, Nagai H, Kondo Y, Misawa N, Toyokuni S. Evaluation of two distinct methods to quantify the uptake of crocidolite fibers by mesothelial cells. *J Clin Biochem Nutr* 2013; **53**: 27–35.
34 Nagai H, Toyokuni S. Differences and similarities between carbon nanotubes and asbestos fibers during mesothelila carcinogenesis. *Cancer Sci* 2012; **103**: 1378–90.
35 Toyokuni S. Role of iron in carcinogenesis: cancer as a ferrotoxic disease. *Cancer Sci* 2009; **100**: 9–16.
36 Toyokuni S. Reactive oxygen species-induced molecular damage and its application in pathology. *Pathol Int* 1999; **49**: 91–102.
37 Toyokuni S. Iron and thiols as two major players in carcinogenesis: friends or foes? *Front Pharmacol* 2014; **5**: 200.
38 Toyokuni S, Uchida K, Okamoto K, Hattori-Nakakuki Y, Hiai H, Stadtman ER. Formation of 4-hydroxy-2-nonenal-modified proteins in the renal proximal tubules of rats treated with a renal carcinogen, ferric nitrilotriacetate. *Proc Natl Acad Sci USA* 1994; **91**: 2616–20.
39 Toyokuni S, Sagripanti J-L. DNA single- and double-strand breaks produced by ferric nitrilotriacetate in relation to renal tubular carcinogenesis. *Carcinogenesis* 1993; **14**: 223–7.
40 Toyokuni S, Sagripanti J-L. Association between 8-hydroxy-2′-deoxyguanosine formation and DNA strand breaks mediated by copper and iron. *Free Radic Biol Med* 1996; **20**: 859–64.
41 Toyokuni S. Mysterious link between iron overload and CDKN2A/2B. *J Clin Biochem Nutr* 2011; **48**: 46–9.
42 Akatsuka S, Yamashita Y, Ohara H *et al.* Fenton reaction induced cancer in wild type rats recapitulates genomic alterations observed in human cancer. *PLoS One* 2012; **7**: e43403.

Supporting Information

Additional supporting information may be found in the online version of this article:

Fig. S1. Amounts of adsorbed protein.

Fig. S2. Neither hemoglobin nor transferrin increases the fluorescence intensity of RhoNox-1.

Table S1. Summary table of characteristics of multi-wall carbon nanotubes (MWCNT).

Table S2. List of in-solution digestion results.